ACS APPLIED MATERIALS & INTERFACES

Article

Highly Stretchable and Conductive Copper Nanowire Based Fibers with Hierarchical Structure for Wearable Heaters

Yin Cheng, Hange Zhang, Ranran Wang, Xiao Wang, Haitao Zhai, Tao Wang, Qinghui Jin, and Jing Sun

ACS Appl. Mater. Interfaces, **Just Accepted Manuscript** • DOI: 10.1021/acsami.6b09293 • Publication Date (Web): 21 Sep 2016

Just Accepted

ACS Publications

ACS Applied Materials & Interfaces is published by the American Chemical Society.
1155 Sixteenth Street N.W., Washington, DC 20036

Highly Stretchable and Conductive Copper Nanowire Based Fibers with Hierarchical Structure for Wearable Heaters

Yin Cheng,[†,#] Hange Zhang,[‡,#] Ranran Wang,[,†] Xiao Wang,[†] Haitao Zhai,[†] Tao Wang,[†] Qinghui Jin, [‡] and Jing Sun[*,†]*

[†]State Key Laboratory of High Performance Ceramics and Superfine Microstructure, Shanghai Institute of Ceramics, Chinese Academy of Sciences. Shanghai 200050, China

[‡]State Key Laboratory of Transducers Technology, Shanghai Institute of Microsystem and Information Technology, Chinese Academy of Sciences. Shanghai 200050, China

KEYWORDS: Copper nanowire, composite fiber, heating fabric, stretchable, wearable

ABSTRACT

Wearable heaters have been increasingly attracting researchers' great interest due to its efficient utility in warm-keeping and thermotherapy. Nowadays carbon nanomaterials and metallic nanowires tend to become the mainstream heating elements in wearable heaters considering their

excellent electrical and mechanical properties. Though considerable progress have been made, there still exist challenging issues that need to be addressed in practical applications, including the bad breathability and the poor endurance to mechanical deformations. Here, we devise a copper nanowire based composite fiber with unique hierarchical structure. This fiber possesses not only excellent heating performance, but also fantastic tolerance to mechanical impact, like bending, twisting and stretching. We further weave these fibers into a wearable heating fabric and realize smart personal heating management through an Android phone by integrating with microcontroller unit. Two practical applications are demonstrated including a heating kneepad for articular thermotherapy and a heating coat on an infant model for warm keeping.

INTRODUCTION

Wearable heater, a newly emerging functional device, is mainly devoted to offering human body warm keeping and thermal therapy. Electrically driven resistive heaters are highly suitable for the desired purpose considering the easy processing technique, controllable operation and efficient power conversion. Indium tin oxide (ITO) has been the conventional choice as the key heating element and widely used in heater fabrication. However, due to its ceramic nature of brittleness and ever-rising cost of indium, new promising candidates are in urgent need. Nowadays, as some promising nanomaterials exhibit excellent electrical and mechanical properties, researchers have been increasingly exploiting carbon nanotubes (CNT),[1-6] graphene,[7-10] metallic nanowires,[11-20] or their mixtures[21, 22] as heating elements in resistive heaters, with glasses or polymers as supporting substrates. Most of these heaters are employed in applications as defoggers/defrosters,[1, 4, 7, 9, 10, 12, 14, 15, 17, 18, 22] industrial heating treatment,[5] displays,[6, 16] sensors,[21] and even art conservation,[2, 3] only a limited number of the devices have pioneered their utilization in wearable heaters and achieved encouraging results.[8, 13]

Given the practical application conditions of wearable heaters in warm keeping and thermal therapy, there are two significant factors that deserve special attention. For one thing, the heaters should provide enough breathability to prevent the skin perspiration from accumulating. Otherwise it would cause great discomfort to the wearer. For another, when wearable heaters cover movable parts of human body, human motions would inevitably affect the heaters mechanically, like bending, twisting and even stretching, and this is particularly true in the case of thermal therapy, where the heaters should maintain conformal contact with the movable skin and joints (like back, wrist, and knee) [23-25] to ensure comfort and efficient heat conduction.[26] As such, the heaters are supposed to be capable of enduring frequently imposed mechanical deformations during operation. Some researchers artfully coated solution-processed heating elements, like metallic nanowires[27] and CNT,[11, 28] to fabrics, obtaining wearable heaters. These fabric-based heaters achieved effective heating ability and negligible breathability loss; nevertheless, the deformations like stretching could probably damage the vulnerable conducting network and impair the heating performance. To realize thermal therapy, a brilliant methodology is to configure serpentine metal electrodes on polymer substrates.[29-32] Despite the considerably improved tolerance to deformations, the fabrication still involves complicated processing techniques. Besides, the polymer substrate is not vapor-permeable, which would bring about discomfort during long time wearing.

Here, we proposed a facile and scalable method to fabricate copper nanowire (CuNW) based composite fiber with a unique hierarchical configuration. The composite fiber maintains extremely stable electrical conductivity under bending, twisting and even stretching (resistance increase of 50% at strain of 100%) deformations, enabling it to serve as high performance stretchable heating fiber (SHF). The SHF could be heated from 20 ^{o}C to 57 ^{o}C at a low DC

voltage of 3 V within 20s, and revealed no appreciable performance degradation after various mechanical deformations. We constructed a model to understand the thermodynamic heating response of the SHF well. The SHFs were further weaved into a heating fabric, which inherited the excellent endurance to various deformations and also possessed good breathability. Finally, to achieve a wearable and smart personal heating system (WSPHS), we integrated the heating fabric and microcontroller unit (MCU) into clothes, which realized the interaction between the WSPHS and a smart phone. The WSPHS holds great promise for applications in warm keeping, thermotherapy, especially for movable joint positions and for people with mobility difficulties, like babies, the elderly, and the disabled. To the best of our knowledge, no similar work has been reported yet which features a washable, breathable and deformable heating fabric directly weaved from intrinsically stretchable and conductive composite fibers with hierarchical structure.

RESULTS AND DISCUSSION

Fabrication and morphology characterization of the SHF. We developed a facile and scalable method to fabricate the SHF (detailed process in the Experimental Section). Briefly speaking, CuNWs (Figure S1, Supporting Information) were firstly coated onto a helical yarn which consisted of polyester (PE) microfibers. Then H_2 plasma was implemented to endow the CuNW network with high electrical conductivity. Finally the above structure was dip-coated in liquid silicone rubber and cured to obtain a sealing and protecting layer. This well-designed hierarchical structure of the SHF was schematically demonstrated in Scheme 1. The morphology of the PE yarn was revealed by scanning electron microscope (SEM) in Figure 1a (the top), and its yarn structure was clearly shown in the stretched (strain of 50%) state (the bottom). From Figure 1b, it obviously manifested that the CuNW network coated conformally onto the surface

of the PE yarn (the top) and the PE microfibers (the bottom), indicating the efficient dyeing of CuNW ink through the dip-coating processing.[33, 34] Moreover, the nanowire content and thus the corresponding electrical conductivity (here characterized by "the resistance per unit length" R_n, for simplicity) could be tuned by adjusting the dip-coating times with ease (Figure S2, Supporting Information). The room-temperature hydrogen plasma treatment was utilized to endow the copper nanowire network with high conductivity.[35] The etching and reductive effect of hydrogen plasma helped to remove organic residues and oxide layers on the nanowire surface. Moreover, the confined thermal heating caused by the surface plasmon resonance at the nanowire contact positions led to the local nanowelding (as revealed in Figure 1c) in between adjacent nanowires. Both of the two effects contributed to tremendously decreased contact resistance of the copper nanowire network. At the last procedure of rubber coating, the elastomeric polymer coated uniformly on the outside surface, as seen in Figure 1d, and solid- or hollow-core structured SHF (insets in Figure 1d) could be fabricated through two different coating methods (see Experimental Section), which will be further investigated in the next part. The prepared SHF was highly flexible and stretchable (bottom inset in Figure 1d). Also worth noting is that the solid-core structured SHF was an optimization and improvement of our previous work in terms of structure design,[36] and as a result the solid-core structured SHF not only possessed better electromechanical performance (as seen in Figure S3, also investigated detailedly in the following part), but also eliminated the air gap existence within the fiber via complete permeation of liquid polymer, which solved the problem of localized excessively high temperature distribution during the operation as heaters.

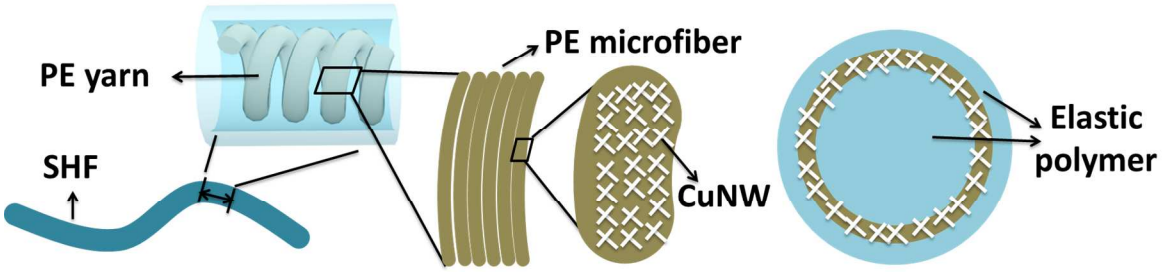

Scheme 1. The schematic illustration of the hierarchical structure of the SHF. Left is the hierarchical description of the SHF structure. Right is the schematic diagram of the cross-section structure.

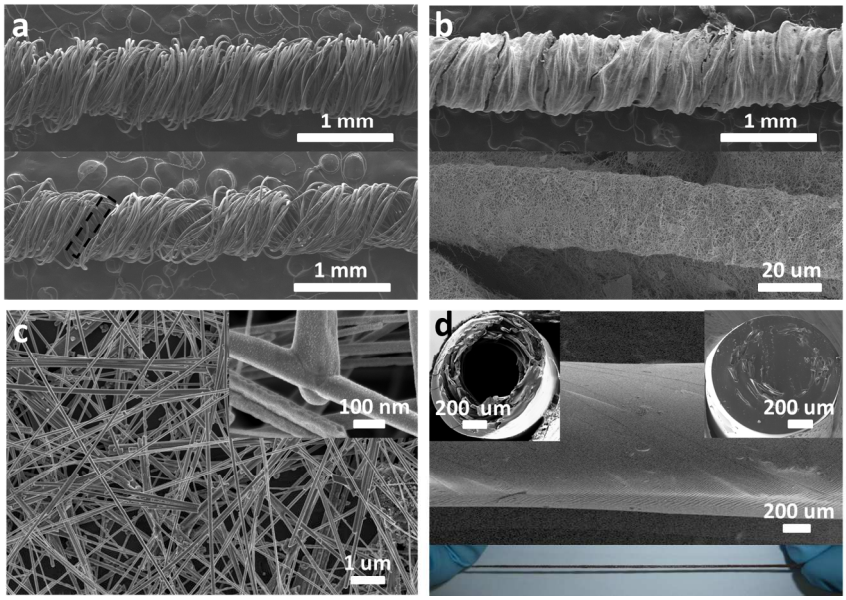

Figure 1. The morphology characterization of the SHF. a) SEM images of the PE yarn before (top) and after (bottom) being stretched to strain of 50%. The dotted box in the bottom image marked the gap position of the PE yarn. b) SEM images of the PE yarn coated with CuNWs (top) and a localized single PE microfiber coated with CuNWs (bottom). c) SEM images of the CuNWs network on the surface of the PE microfiber and the welding junction of two contacting CuNWs (inset). d) SEM images of the SHF and the cross sections of a hollow-core structured SHF (top left inset) and solid-core structured SHF (top right inset). The bottom inset showed a SHF (length of 8 cm).

Electromechanical performance of the SHF. In order to achieve high-performance wearable heaters, the key and also difficult prerequisite is to ensure stable conductivity of the heating element under different mechanical deformations. Here, we investigated the electromechanical performance of the SHF (dip-coated for 6 times in the following part) systematically to confirm its viability as stretchable heaters. Figure 2a displayed the relative resistance variation of three different SHF samples under tensile strain up to 100%: SHF before rubber coating, hollow-core structured SHF after rubber coating, and solid-core structured SHF after rubber coating. We found that the SHF before rubber coating and the hollow-core structured SHF exhibited similar resistance change under stretching, and the resistance increased by a factor of 3 at ultimate strain of 100%. In contrast, the solid-core structured SHF underwent a much smaller degradation of conductivity: the resistance increased by 50% at strain of 100%. To understand this difference, we traced the surface microstructure variation of the SHF before rubber coating during the stretching up to 100% strain (Figure S4, Supporting Information). When the SHF started to be stretched, gaps in between the PE yarns emerged. As the stretching continued, the number of the gaps increased and the size grew larger, both of which accommodated the applied strain. These effects inevitably damaged the conductive CuNW networks at the gap positions, resulting in the resistance increase, as occurred for the SHF before rubber coating and the hollow-core structured SHF. However, in the case of the solid-core structured SHF, the infiltration of liquid polymer during fabrication effectively passivated the gaps, which would then relieve the adverse impact of stretching on the conductive network of the SHF, accounting for its improved tolerance to tensile strain. This solid-core structured SHF showed obvious advantage to other reported stretchable conductors in the maintenance of conductivity against imposed tensile strain: >300% increase of resistance at 30% strain for a

metal deposited PDMS with porous structure,[37] 160% increase of resistance at 100% strain for a PUS-AgNW-PDMS with a binary network design,[38] 150% increase of resistance at 40% strain for a graphene-silver nanowire hybrid foam,[39] as comparisons with our work (50% increase of resistance at 100% strain). Note that the solid-core structured SHF was selected for further investigation in the following. Figure 2b described the resistance change of SHF under the bending test. The results suggested that the bending barely impact the conductive network of the SHF: the relative resistance increase was within 2% even at a bending radius of 1 mm. Next, we conducted the twisting test to the SHF. Both the clockwise and counterclockwise twisting, up to 100 turns per meter, led to negligible resistance increase (within 4%) as seen in Figure 2c. We believe the particularly stable conductivity of the SHF under bending and twisting deformations is due to the enhanced anchoring of the CuNW networks onto the PE microfibers by virtue of the rubber coating. At last, cyclic testing was implemented to evaluate the durability of the SHF under various mechanical deformations. As seen in Figure 2d, after 1000 cycles of stretching (strain of 50%), bending (radius of 1 mm), and twisting (50 turns per meter), the relative resistance increase were 5%, 2% and 2.5%, respectively. The excellent mechanical robustness and superb endurance to deformations of SHF guaranteed its reliability in the utilization of wearable heating materials.

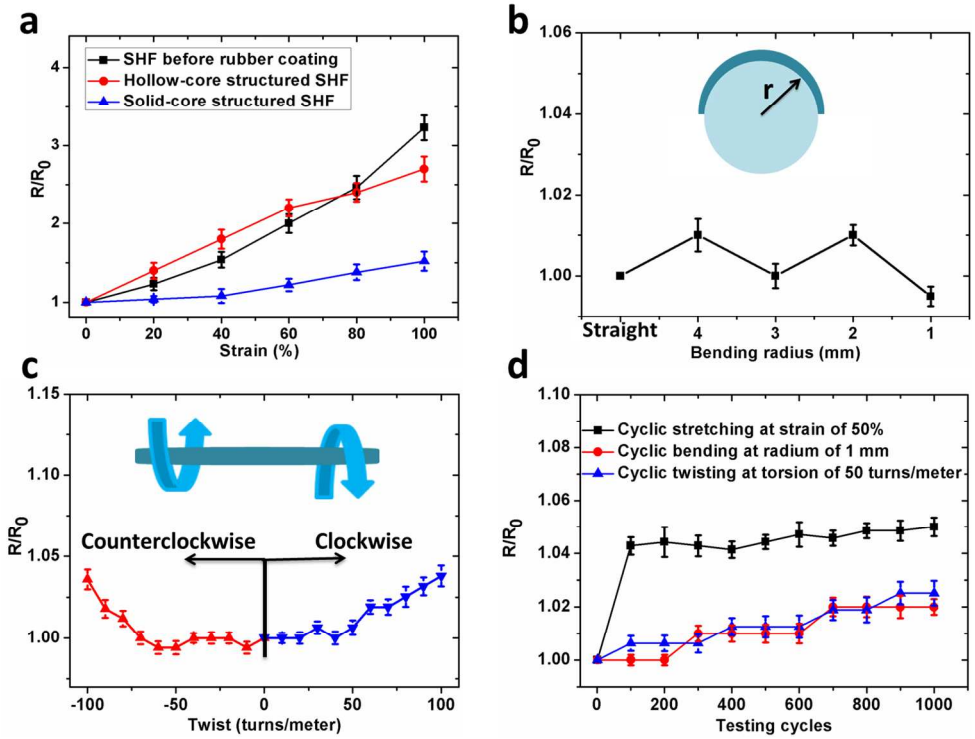

Figure 2. Electromechanical properties of the SHF. a) The relative resistance variation of SHF before rubber coating, hollow-core structured SHF after rubber coating, and solid-core structured SHF after rubber coating. b) The relative resistance variation of SHF under the bending from straight to bending radius of 1mm. The schematic inset depicted the SHF wrapping tightly around a cylinder in bending test. c) The relative resistance variation of the SHF under the twisting up to -100 turns/meter (counterclockwise direction) and to100 turns/meter (clockwise direction). The schematic inset depicted the SHF twisted in the counterclockwise direction. d) The relative resistance variation of the SHF in cyclic stretching (strain of 50%), bending (bending radius of 1mm) and twisting (torsion of 50 turns/meter) up to 1000 cycles.

Thermodynamic analysis of the heating response of the SHF. To evaluate the heating performance of the SHF, its temperature was captured in real-time with the aid of an infrared (IR) thermal camera at a certain input DC voltage. For a specific SHF sample (l=8 cm, r=0.5 mm, R_n=2.5 Ω/cm), when a constant voltage was applied, as shown in Figure 3a, the temperature rose

quickly and reached a steady plateau within 20s due to the Joule heating of the conductive percolated CuNW network. Also, higher DC voltage input led to higher saturation temperature (T_{sat}). T_{sat} could be as high as 57 ^{o}C under a low voltage of 3V. To reveal the dependence of heating performance on the geometrical size of the SHF, the time-dependent temperature curves of a SHF (l=2 cm, R_n=2.5 Ω/cm) at constant input voltage (0.9V) were measured in Figure 3b, while increasing its radius by repeated coating and curing of rubber layer. Clearly, as the diameter of the SHF increased, the T_{sat} lowered. Besides, the heating time needed to reach the T_{sat} grew longer. In addition, cyclic heating test was implemented as seen in Figure 3c. A constant voltage (3V) was repeatedly applied on the SHF (l=8 cm, r=0.5 mm, R_n=2.5 Ω/cm), and the T_{sat} remained almost unchanged even after 100 heating cycles, suggesting its excellent durability as heating material.

In order to understand mechanism underlying the heating behavior, we conducted a thermodynamic analysis of the heating response of the SHF (see detailed analysis in Supporting Information). When the applied voltage caused Joule heating, it partly contributed to the temperature rise of the SHF, and also dissipated into the ambient environment in forms of radiation and convection heat loss. Based on this energy balance principle, we established an equation:

$$\frac{U^2}{R} = C \cdot \frac{dT}{dt} + A \cdot \varepsilon \cdot \sigma \cdot \left(T^4 - {T_0}^4\right) + A \cdot h_C \cdot (T - T_0) \quad (1)$$

Where the left part is the Joule heating power; the items in the right represent the heat storage rate of the SHF, the radiation and convective heat loss rate, respectively. Here U refers to the applied DC voltage, R the electrical resistance of the SHF, t the heating time, C the heat capacity of the material, A the surface area of the SHF, ε the material's emissivity, σ the Stefan-Boltzmann constant, T the instantaneous temperature of the SHF, T_0 the initial ambient

temperature, h_C the convective heat transfer coefficient. By solving this differential equation, we could obtain the expressions of the time-dependent temperature T, the time constant τ, and the T_{sat} of the SHF in equations (2-4), respectively.

$$T = T_0 + \frac{U^2}{RhA} \cdot (1 - e^{-\frac{t}{\tau}}) \quad (2)$$

$$\tau = \frac{\rho_2 c_2}{2h} \cdot r \quad (3)$$

$$T_{sat} = T_0 + \frac{1}{2\pi h} \cdot \frac{U^2}{R_n l^2 r} \quad (4)$$

Here, h refers to the total heat transfer coefficient, ρ_2 and c_2 the density and specific heat capacity of the rubber layer, r and l the radius and length of the SHF, R_n the normalized resistance of the SHF.

As a result, we could make rational expectations about the heating performance of the SHF: first, the heating time needed to reach saturation lasts longer with the increase of the radius of the SHF; second, the saturation temperature is affected by several parameters collectively, and for a specific SHF sample, the applied voltage determines the ultimate saturation temperature in a quadratic relationship. We further extracted the relationship of the saturation temperature versus the applied voltage for a specific SHF from Figure 3a, the time constant and saturation temperature at a constant input voltage to the radius from Figure 3b, as displayed in Figure 3d-f. Good linear fitting was observed for $T_{sat} \sim U^2$, $\tau \sim r$ and $T_{sat} \sim \frac{1}{r}$. The experimental results coincided well with the modeling expectations, confirming the validity of the above mechanism analysis.

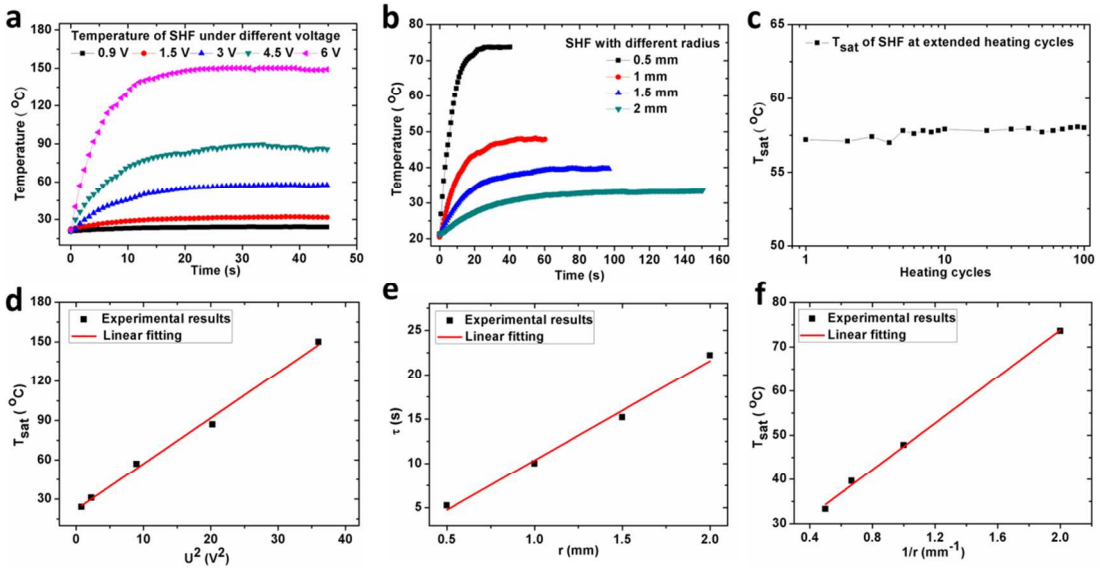

Figure 3. The heating performance of the SHF and the thermodynamic analysis. a) The time-dependent temperature curves of the SHF under different constant DC voltages from 0.9V to 6V. b) The time-dependent temperature curves of the SHF with different radius (from 0.5 mm to 2 mm) under constant DC voltage of 0.9V. c) The saturation temperature variation of the SHF at extended heating cycles under DC voltage of 3V. d) The experimental results of T_{sat}~U^2 (extracted from Figure 3a) and the linear fitting. e) The experimental results of τ~r (extracted from Figure 3b) and the linear fitting. f) The experimental results of T_{sat}~$\frac{1}{r}$ (extracted from Figure 3b) and the linear fitting.

Heating performance of the SHF under various mechanical deformations. As wearable heaters in daily life would unavoidably suffer mechanical impacts during human body movements, especially at the joint positions for articular thermal therapy, it is absolutely essential to evaluate the heating performance of the SHF when subjected to mechanical deformations. Figure 4a recorded the temperature variation curves of a SHF (l=6 cm, r=0.5 mm), which was first heated to specific temperatures at constant DC voltages (53 ^{o}C at 2V, 66 ^{o}C at 2.5V) and then stretched to step strains of 20%, 40%, and 80% consecutively. The results

demonstrated that the SHF continued working stably though the imposed tensile strains led to a corresponding heating temperature decrease. Specifically, at strain of 40%, the heating temperatures of SHF decreased only a little bit, from 53 ^{o}C and 66 ^{o}C to 46 ^{o}C and 61 ^{o}C, respectively. These results were much better compared with a wearable AgNW/PDMS film heater,[13] where a strain of 30% caused a temperature decrease from ~57 ^{o}C and ~70 ^{o}C to ~40 ^{o}C and ~45 ^{o}C. This advantage stemmed from the superb resistance stability of solid-core structured SHF under tensile strain: only a resistance increase of 4% and 8% at strains of 20% and 40% (Figure 2a), respectively. While the strain increased to 80%, the heating temperature descended to 33 ^{o}C and 47 ^{o}C. An alternative strategy to offset the temperature decline is to raise the DC voltage, under the guidance of equation (4).

We further took IR thermal images of a SHF under different kinds of deformations. As compared with the original state (Figure 4b), the heating temperature of the SHF went through imperceptible change under bending (Figure 4c) and twisting (Figure 4d) deformations, owing to its exceptionally stable electrical conductance on these conditions (as testified in Figure 2b-c). Figure 4e displayed that a slight temperature drop occurred when the SHF was stretched to strain of 50%, consistent with the results in Figure 4a. Also note that the SHF could offer continuous heating during the whole stretching-releasing process (Movie S1, Supporting Information).

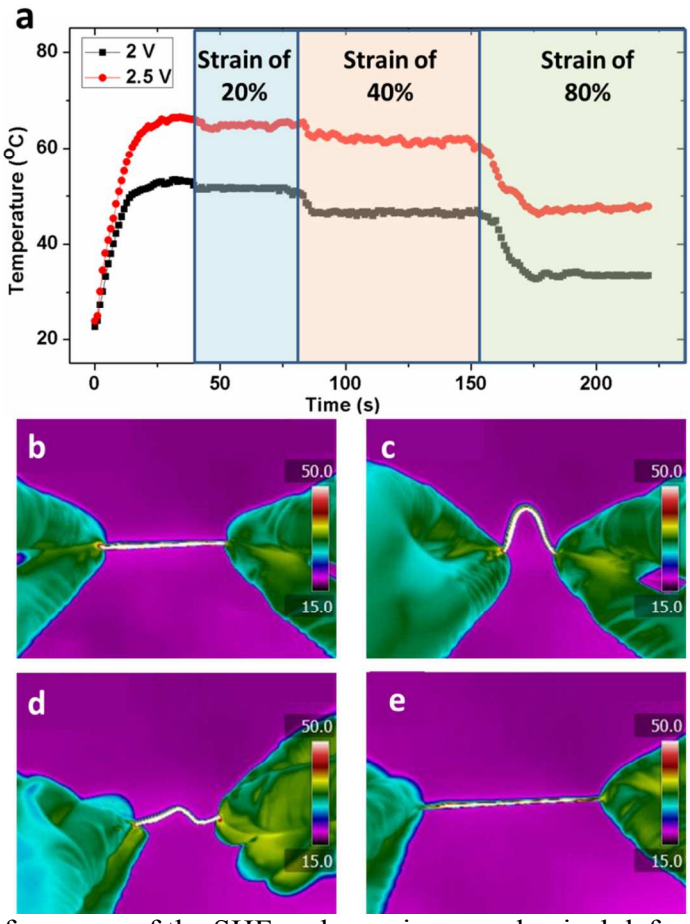

Figure 4. Heating performance of the SHF under various mechanical deformations. a) Time-dependent temperature curves of a SHF being stretched to strain of 20%, 40% and 80% consecutively under DC voltages of 2V and 2.5V. b) IR thermal image of a SHF (l=4 cm, r=0.5 mm) at original state (straight) under constant voltage of 1.2V. c) IR thermal image of the SHF at bending state. d) IR thermal image of the SHF at twisting state. e) IR thermal image of the SHF at stretching (strain of 50%) state.

The integration of the SHFs into the WSPHS. To demonstrate the feasibility of the SHF in wearable applications, we weaved the SHFs into a heating fabric, and then integrate it with clothes and MCU, resulting in a WSPHS controlled by a smart phone, as illustrated in the process schematic (Figure 5a, detailed information in Experimental Section). Figure 5b (inset)

showed a heating fabric made from weaving the SHFs and the temperature distribution on the heating fabric (DC voltage of 1.8V) was fairly uniform. The heating fabric also inherited the flexibility and provided enough breathability due to the weaving structure compared with other film-structured wearable heaters (Figure S5, Supporting Information). Additionally, to evaluate the washability of the heating fabric, a repeated washing test (Experimental Section) was carried out, and no obvious heating performance degradation of the heating fabric was found after 40 times washing (Figure S6, Supporting Information). Figure 5c depicted the operation process of the WSPHS (detailed information in Supporting Information): the MCU read the body temperature through the temperature sensor and transmitted it to the Android phone wirelessly with the aid of a Bluetooth module; the user sent the controlling signal to the MCU wirelessly through the Android phone to adjust the output DC voltage applied on the heating fabric, thus regulating the heating temperature as needed. This integration made the wearable heater more portable, convenient, and user-friendly for daily use.[31] As practical application demonstrations, the wearable heating fabrics were fixed onto a kneepad at knee position of a human body (Figure 5d) and a coat at chest position of an infant model (Figure 5g). From the IR thermal images before (Figure 5e, h) and after (Figure 5f, i) switching on the device, the heating fabric effectively heated the corresponding positions, indicating the viable applications in wearable articular thermotherapy and warm keeping. The especially stable electrical conductivity ensured the effective operation of the heating fabric for articular thermotherapy even when the wearer was in motion, for example, knee flexion&extension (Movie S2, Supporting Information). Figure 5j showed the software interface on an android phone which mainly included the real-time body temperature monitoring and heating temperature controlling. The software helped to read the body temperature of the wearer (the infant model in this case, Movie S3, Supporting

Informmation), which ensured safety in use. This WSPHS holds great application promise in articular thermotherapy, where frequent mechanical deformations are involved during human body movements, and in warm-keeping for people, especially ones with mobility problems, like babies, the elderly, and the disabled.

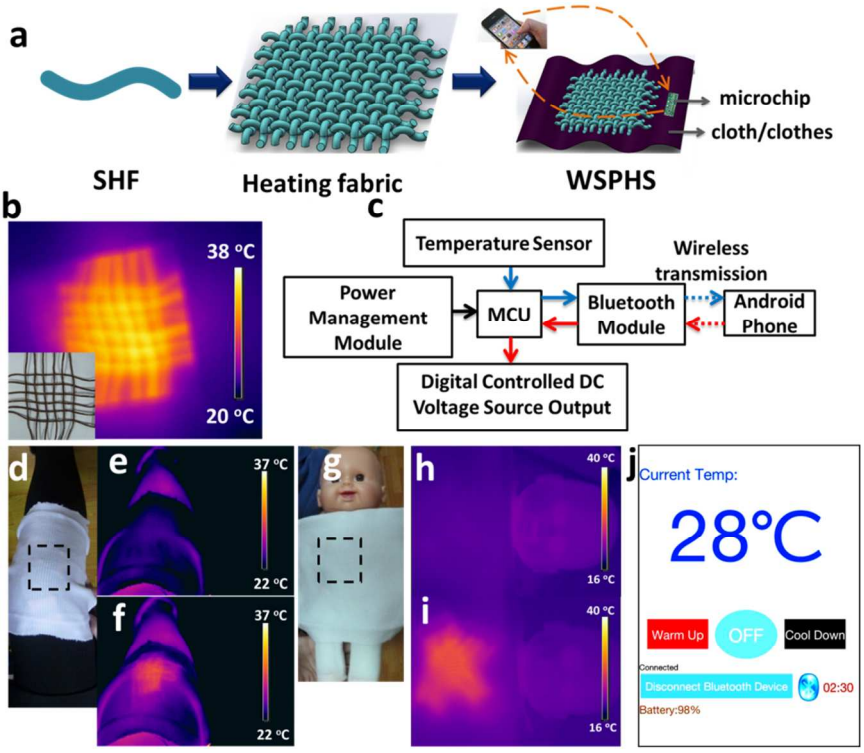

Figure 5. The integration of SHF into WSPHS and the practical wearable applications. a) Process schematic of the integration of WSPHS: weaving SHFs into heating fabric and then integrating the heating fabric with cloth/clothes and a microcontroller chip. b) The IR thermal image of the heating fabric under DC voltage of 1.8V and the photo of the heating fabric (12 SHFs weaved in a cross pattern). c) The schematic illustration of the operation process of the WSPHS. d) The photo of the WSPHS application at the knee position (marked by the dotted box) of a human body. IR thermal images before e) and after f) switching on the device (DC voltage of 1.4V). g) The photo of the WSPHS application at the chest position (marked by the dotted box) of an infant model. IR thermal images before h) and after i) switching on the device (DC voltage

of 1.4V). j) The software interface on an android phone which read the body temperature and controlled the heating temperature.

CONCLUSION

In our work, we have made a successful combination of new material (copper nanowire and yarns), unique structure (solid-core structured composite fiber with hierarchical configuration), and microelectronics (a wearable and smart personal heating system capable of remote monitoring and controlling through a cellphone). We also achieved a breakthrough in high maintenance of conductivity under stretching for stretchable and conductive fiber (resistance increase of 8% at strain of 40%), realized rapid heating under low voltage (from 20 ^{o}C to 57 ^{o}C at a DC voltage of 3 V within 20s), modeled the heat transfer process and analyzed the critical parameters for heating performance in depth. The practical application of the WSPHS is successfully demonstrated by heating up knee position of a human body as articular thermotherapy and chest position of an infant model as warm keeping.

Experimental section

The fabrication process of the SHF: A modified solvothermal method was adopted to synthesize CuNWs.[40, 41] After washing with toluene and transferring into ethanol, a high concentration of CuNW dispersion (30mg/ml) was obtained. The PE yarn (diameter of ~ 700 um), consisting of a bunch of PE microfibers (diameter of 20-25 um), was dipped into the CuNW dispersion and then dried in air. Repeat the dip-coating process to increase the CuNWs content on the PE yarn. After that, the PE yarn with CuNWs coating was treated in H_2 plasma for 10 min. Lastly, the PE yarn with CuNWs coating was dipped into (leaving the two ends out for electrical

connecting) a liquid silicon rubber precursor from a 1A:1B mixture by weight (Ecoflex 00-30, Smooth-On, Inc.) and then cured in oven (100 ^{o}C, 10 min). During this rubber coating processing, the PE yarn could either be stretched to about 50% to allow the infiltration of liquid rubber precursor into the inner hollow space to obtain a solid-core structured SHF, or just coated by liquid rubber precursor on the outside surface to obtain a hollow-core structured SHF. Note that, the polymer coating on the outside surface caused a resistance increase of about 10-20%; the polymer infiltration of the stretched sample led to a resistance increase to 3 times.

The integration of SHFs into WSPHS: The heating fabric was first weaved from 12 SHFs (l=8 cm, r=0.5 mm, R_n=2.5 Ω/cm) in a cross pattern (pitch size of 0.5cm). Then copper wires (2 μm in diameter) were connected to the two ends of the SHFs as external electrodes with the help of conductive copper tape and silver paste. The heating fabric was connected to the digital controlled DC voltage source output module on the microchip controlled by the MCU with all the SHFs in a parallel manner. At last, the heating fabric and microchip were fixed onto various clothes, in this paper, the kneepad and a coat for an infant model, with the aid of medical tapes.

Testing of the washability of the heating fabric: The heating fabric was soaked into water and cleaned ultrasonically for 10min. After the cleaning, the heating fabric was dried with a blower. A DC voltage of 1.8V was applied on the heating fabric, and the saturation temperature of the heating fabric was read from the time-dependent temperature curves recorded by an IR camera. Repeat this process and obtain the saturation temperature variation along with the washing times.

Characterization: The SEM characterization was accomplished using a Hitachi SU8200 FE-SEM. In the testing relative resistance variation along with the strain, the strain loading was implemented with a high-precision motorized linear stage (displacement resolution of 2.5 μm)

and the electrical resistance was recorded with a FLUKE-15B digital multimeter. In the bending test, the SHF (l=2 cm, r=0.5 mm, R_n=2.5 Ω/cm) was wrapped tightly around a cylinder with different radius and measured the relative resistance variation. In the twisting test, the SHF (l=8 cm, r=0.5 mm, R_n=2.5 Ω/cm) was twisted through a high-precision motorized rotation stage (angle resolution of 0.0025°). The time-dependent temperature curves and the IR thermal images were obtained by an IR thermal camera.

ASSOCIATED CONTENT

Supporting Information. Detailed thermodynamic analysis of the heating response of the SHF, detailed information of the WSPHS, Figure S1-S8, Supporting movie S1-S3. This material is available free of charge via the Internet at http://pubs.acs.org.

AUTHOR INFORMATION

Corresponding Authors

*E-mail: (R.W.) wangranran@mail.sic.ac.cn.

*E-mail: (J.S.) jingsun@mail.sic.ac.cn.

Author Contributions

The manuscript was written through contributions of all authors. All authors have given approval to the final version of the manuscript. # These authors contributed equally.

Notes

The authors declare no competing financial interest.

ACKNOWLEDGMENT

This work was financially supported by the National Basic Research Program of China (2012CB932303), the National Natural Science Foundation of China (Grant No.61301036), Shanghai Municipal Natural Science Foundation (Grant No. 13ZR1463600 and 13XD1403900) and The Innovation Project of Shanghai Institute of Ceramics.

REFERENCES

[1] Jang, H.-S.;Jeon, S. K.; Nahm, S. H. The Manufacture of A Transparent Film Heater by Spinning Multi-Walled Carbon Nanotubes. *Carbon* **2011**, *49*, 111-116.

[2] Markevicius, T.;Furferi, R.;Olsson, N.;Meyer, H.;Governi, L.;Carfagni, M.;Volpe, Y.; Hegelbach, R. Towards the Development of A Novel CNTs-Based Flexible Mild Heater for Art Conservation. *Nanomater. Nanotechnol.* **2014**, *4*.

[3] Markevicius, T.; Olsson, N.; Furferi, R.; Meyer, H. Flexible Mild Heaters in Structural Conversation of Paintings State of the Art and Conceptual Design of A New Carbon Nanotubes-Based Heater. *J. Appl. Sci.* **2012**, *12*, 211-220.

[4] Yoon, Y. H.;Song, J. W.;Kim, D.;Kim, J.;Park, J. K.;Oh, S. K.; Han, C. S. Transparent Film Heater Using Single-Walled Carbon Nanotubes. *Adv Mater* **2007**, *19*, 4284-4287.

[5] Janas, D.; Koziol, K. K. Rapid Electrothermal Response of High-Temperature Carbon Nanotube Film Heaters. *Carbon* **2013**, *59*, 457-463.

[6] Liu, P.;Liu, L.;Jiang, K.; Fan, S. Carbon-Nanotube-Film Microheater on a Polyethylene Terephthalate Substrate and Its Application in Thermochromic Displays. *Small* **2011**, *7*, 732-736.

[7] Bae, J. J.;Lim, S. C.;Han, G. H.;Jo, Y. W.;Doung, D. L.;Kim, E. S.;Chae, S. J.;Huy, T.

Q.;Van Luan, N.; Lee, Y. H. Heat Dissipation of Transparent Graphene Defoggers. *Adv Funct Mater* **2012**, *22*, 4819-4826.

[8] Choi, M. K.;Park, I.;Kim, D. C.;Joh, E.;Park, O. K.;Kim, J.;Kim, M.;Choi, C.;Yang, J.;Cho, K. W.;Hwang, J.-H.;Nam, J.-M.;Hyeon, T.;Kim, J. H.; Kim, D.-H. Thermally Controlled, Patterned Graphene Transfer Printing for Transparent and Wearable Electronic/Optoelectronic System. *Adv Funct Mater* **2015**, *25*, 7109-7118.

[9] Kang, J.;Kim, H.;Kim, K. S.;Lee, S. K.;Bae, S.;Ahn, J. H.;Kim, Y. J.;Choi, J. B.; Hong, B. H. High-Performance Graphene-Based Transparent Flexible Heaters. *Nano Lett* **2011**, *11*, 5154-5158.

[10] Sui, D.;Huang, Y.;Huang, L.;Liang, J.;Ma, Y.; Chen, Y. Flexible and Transparent Electrothermal Film Heaters Based on Graphene Materials. *Small* **2011**, *7*, 3186-3192.

[11] Ilanchezhiyan, P.;Zakirov, A. S.;Kumar, G. M.;Yuldashev, S. U.;Cho, H. D.;Kang, T. W.; Mamadalimov, A. T. Highly Efficient CNT Functionalized Cotton Fabrics for Flexible/Wearable Heating Applications. *RSC Adv.* **2015**, *5*, 10697-10702.

[12] Ghosh, D. S.;Chen, T. L.;Mkhitaryan, V.; Pruneri, V. Ultrathin Transparent Conductive Polyimide Foil Embedding Silver Nanowires. *ACS Appl Mater Interfaces* **2014**, *6*, 20943-20948.

[13] Hong, S.;Lee, H.;Lee, J.;Kwon, J.;Han, S.;Suh, Y. D.;Cho, H.;Shin, J.;Yeo, J.; Ko, S. H. Highly Stretchable and Transparent Metal Nanowire Heater for Wearable Electronics Applications. *Adv Mater* **2015**, *27*, 4744-4751.

[14] Kim, T.;Kim, Y. W.;Lee, H. S.;Kim, H.;Yang, W. S.; Suh, K. S. Uniformly Interconnected Silver-Nanowire Networks for Transparent Film Heaters. *Adv Funct Mater* **2013**, *23*, 1250-1255.

[15] Kim, H.-J.;Kim, Y.;Jeong, J.-H.;Choi, J.-H.;Lee, J.; Choi, D.-G. A Cupronickel-Based Micromesh Film for Wse as A High-Performance and Low-Voltage Transparent Heater. *J. Mater. Chem. A* **2015**, *3*, 16621-16626.

[16] Celle, C.;Mayousse, C.;Moreau, E.;Basti, H.;Carella, A.; Simonato, J.-P. Highly Flexible Transparent Film Heaters Based on Random Networks of Silver Nanowires. *Nano Res* **2012**, *5*, 427-433.

[17] Chen, J.;Chen, J.;Li, Y.;Zhou, W.;Feng, X.;Huang, Q.;Zheng, J. G.;Liu, R.;Ma, Y.; Huang, W. Enhanced Oxidation-Resistant Cu-Ni Core-Shell Nanowires: Controllable One-Pot Synthesis and Solution Processing to Transparent Flexible Heaters. *Nanoscale* **2015**, *7*, 16874-16879.

[18] Ji, S.;He, W.;Wang, K.;Ran, Y.; Ye, C. Thermal Response of Transparent Silver Nanowire/PEDOT:PSS Film Heaters. *Small* **2014**, *10*, 4951-4960.

[19] Ding, S.; Jiu, J.; Gao, Y.; Tian, Y.; Araki, T.; Sugahara, T.; Nagao, S.; Nogi, M.; Koga, H.; Suganuma, K.; Uchida, H. One-Step Fabrication of Stretchable Copper Nanowire Conductors by A Fast Photonic Sintering Technique and Its Application in Wearable Devices. *ACS Appl Mater Interfaces* **2016**, *8*, 6190-6199.

[20] Kumar, D.; Woo, K.; Moon, J. Promising Wet Chemical Strategies to Synthesize Cu Nanowires for Emerging Electronic Applications. *Nanoscale* **2015**, *7*, 17195-17210.

[21] Kim, D.;Zhu, L.;Jeong, D.-J.;Chun, K.;Bang, Y.-Y.;Kim, S.-R.;Kim, J.-H.; Oh, S.-K. Transparent Flexible Heater Based on Hybrid of Carbon Nanotubes and Silver Nanowires. *Carbon* **2013**, *63*, 530-536.

[22] Zhang, X.;Yan, X.;Chen, J.; Zhao, J. Large-Size Graphene Microsheets as A Protective Layer for Transparent Conductive Silver Nanowire Film Heaters. *Carbon* **2014**, *69*, 437-

443.

[23] Michlovitz, S.;Hun, L.;Erasala, G. N.;Hengehold, D. A.; Weingand, K. W. Continuous Low-Level Heat Wrap Therapy is Effective for Treating Wrist Pain. *Arch. Phys. Med. Rehabil.* **2004**, *85*, 1409-1416.

[24] Petrofsky, J. S.;Laymon, M.; Lee, H. Effect of Heat and Cold on Tendon Flexibility and Force to Flex the Human Knee. *Med. Sci. Monit.* **2013**, *19*, 661-667.

[25] Nadler, S. F.;Steiner, D. J.;Erasala, G. N.;Hengehold, D. A.;Hinkle, R. T.;Goodale, M. B.;Abeln, S. B.; Weingand, K. W. Continuous Low-Level Heat Wrap Therapy Provides More Efficacy than Ibuprofen and Acetaminophen for Acute Low Back Pain. *Spine* **2002**, *27*, 1012-1017.

[26] Kim, D. H.;Lu, N.;Ma, R.;Kim, Y. S.;Kim, R. H.;Wang, S.;Wu, J.;Won, S. M.;Tao, H.;Islam, A.;Yu, K. J.;Kim, T. I.;Chowdhury, R.;Ying, M.;Xu, L.;Li, M.;Chung, H. J.;Keum, H.;McCormick, M.;Liu, P.;Zhang, Y. W.;Omenetto, F. G.;Huang, Y.;Coleman, T.; Rogers, J. A. Epidermal Electronics. *Science* **2011**, *333*, 838-843.

[27] Hsu, P. C.;Liu, X.;Liu, C.;Xie, X.;Lee, H. R.;Welch, A. J.;Zhao, T.; Cui, Y. Personal Thermal Management by Metallic Nanowire-Coated Textile. *Nano Lett* **2015**, *15*, 365-371.

[28] Rahman, M. J.; Mieno, T. Conductive Cotton Textile from Safely Functionalized Carbon Nanotubes. *J Nanomater* **2015**, *2015*, 1-10.

[29] Webb, R. C.;Bonifas, A. P.;Behnaz, A.;Zhang, Y.;Yu, K. J.;Cheng, H.;Shi, M.;Bian, Z.;Liu, Z.;Kim, Y.-S.;Yeo, W.-H.;Park, J. S.;Song, J.;Li, Y.;Huang, Y.;Gorbach, A. M.; Rogers, J. A. Ultrathin Conformal Devices for Precise and Continuous Thermal Characterization of Human Skin. *Nat Mater* **2013**, *12*, 1078-1078.

[30] Son, D.;Lee, J.;Qiao, S.;Ghaffari, R.;Kim, J.;Lee, J. E.;Song, C.;Kim, S. J.;Lee, D. J.;Jun, S.

W.;Yang, S.;Park, M.;Shin, J.;Do, K.;Lee, M.;Kang, K.;Hwang, C. S.;Lu, N.;Hyeon, T.; Kim, D.-H. Multifunctional Wearable Devices for Diagnosis and Therapy of Movement Disorders. *Nat Nanotechnol* **2014**, *9*, 397-404.

[31] Choi, S.;Park, J.;Hyun, W.;Kim, J.;Kim, J.;Lee, Y. B.;Song, C.;Hwang, H. J.;Kim, J. H.;Hyeon, T.; Kim, D.-H. Stretchable Heater Using Ligand-Exchanged Silver Nanowire Nanocomposite for Wearable Articular Thermotherapy. *Acs Nano* **2015**, *9*, 6626-6633.

[32] Kim, J.;Lee, M.;Shim, H. J.;Ghaffari, R.;Cho, H. R.;Son, D.;Jung, Y. H.;Soh, M.;Choi, C.;Jung, S.;Chu, K.;Jeon, D.;Lee, S. T.;Kim, J. H.;Choi, S. H.;Hyeon, T.; Kim, D. H. Stretchable Silicon Nanoribbon Electronics for Skin Prosthesis. *Nat Commun* **2014**, *5*, 5747.

[33] Hu, L.;Pasta, M.;Mantia, F. L.;Cui, L.;Jeong, S.;Deshazer, H. D.;Choi, J. W.;Han, S. M.; Cui, Y. Stretchable, Porous, and Conductive Energy Textiles. *Nano Lett* **2010**, *10*, 708-714.

[34] Kang, T. J.;Choi, A.;Kim, D.-H.;Jin, K.;Seo, D. K.;Jeong, D. H.;Hong, S.-H.;Park, Y. W.; Kim, Y. H. Electromechanical Properties of CNT-Coated Cotton Yarn for Electronic Textile Applications. *Smart Mater. Struct.* **2011**, *20*, 015004.

[35] Wang, R.; Zhai, H.; Wang, T.; Wang, X.; Cheng, Y.; Shi, L.; Sun, J. Plasma-Induced Nanowelding of A Copper Nanowire Network and Its Application inTransparent Electrodes and Stretchable Conductors. *Nano Res* **2016**, *9*, 2138–2148.

[36] Cheng, Y.; Wang, R.; Sun, J.; Gao, L. Highly Conductive and Ultrastretchable Electric Circuits from Covered Yarns and Silver Nanowires. *ACS nano* **2015**, *9*, 3887-3895.

[37] Jeong, G. S.;Baek, D. H.;Jung, H. C.;Song, J. H.;Moon, J. H.;Hong, S. W.;Kim, I. Y.; Lee, S. H. Solderable and Electroplatable Flexible Electronic Circuit on A porous Stretchable Elastomer. *Nat Commun* **2012**, *3*, 977.

[38] Ge, J.;Yao, H. B.;Wang, X.;Ye, Y. D.;Wang, J. L.;Wu, Z. Y.;Liu, J. W.;Fan, F. J.;Gao, H.

L.;Zhang, C. L.; Yu, S. H. Stretchable Conductors Based on Silver Nanowires: Improved Performance Through A Binary Network Design. *Angew Chem Int Ed Engl* **2013**, *52*, 1654-1659.

[39] Wu, C.;Fang, L.;Huang, X.; Jiang, P. Three-Dimensional Highly Conductive Graphene-Silver Nanowire Hybrid Foams for Flexible and Stretchable Conductors. *ACS Appl Mater Interfaces* **2014**, *6*, 21026-21034.

[40] Zhang, D.;Wang, R.;Wen, M.;Weng, D.;Cui, X.;Sun, J.;Li, H.; Lu, Y. Synthesis of Ultralong Copper Nanowires for High-Performance Transparent Electrodes. *J Am Chem Soc* **2012**, *134*, 14283-14286.

[41] Cheng, Y.;Wang, S.;Wang, R.;Sun, J.; Gao, L. Copper Nanowire Based Transparent Conductive Films with High Stability and Superior Stretchability. *J Mater Chem C* **2014**, *2*, 5309.

TOC